

Received November 15, 2018, accepted November 28, 2018, date of publication December 4, 2018,
date of current version December 31, 2018.

Digital Object Identifier 10.1109/ACCESS.2018.2884710

Identifying Individual Camera Device From RAW Images

TONG QIAO¹ AND FLORENT RETRAINT²

¹School of Cyberspace, Hangzhou Dianzi University, Hangzhou 310018, China

²ICD, UMR 6281 CNRS, University of Technology of Troyes, 10300 Troyes, France

Corresponding author: Tong Qiao (tong.qiao@hdu.edu.cn)

This work was supported in part by the Natural Science Foundation of China under Grant 61702150, in part by the Public Research Project of Zhejiang Province under Grant LGG19F020015, in part by the China Scholarship Council Program, and in part by the ANR Project DEFACTO ANR-16-DEFA-0002.

ABSTRACT This paper investigates the problem of identifying the individual imaging device source of the same model from a natural image in RAW format. We propose an enhanced Poissonian–Gaussian model describing the distribution of pixels from a RAW image. The parameters of this statistical noise model are considered as unique fingerprints and, hence, used to identify the source camera device. The source camera identification problem is cast within the framework of the hypothesis testing theory. In an ideal context, where all model parameters are perfectly known, the Likelihood Ratio Test (LRT) is presented, and its performance is theoretically established. The statistical performance of this optimal LRT serves as an upper bound for the detection power. For a practical use, when the nuisance parameters are unknown, a generalized LRT based on estimation of those parameters is designed to deal with unknown expectation of pixels (roughly, the image content). More importantly, by combining multiple sub classifiers together with the voting strategy, a multi-classifier is proposed to identify multiple individual devices. Numerical results on simulated data and on various large dataset of real natural images highlight the relevance of our proposed approach.

INDEX TERMS Digital forensics, source device identification, noise models, nuisance parameters, hypothesis testing.

I. INTRODUCTION AND CONTRIBUTIONS

Digital image forensics is a new technique aiming at collecting digital evidence, such as identifying the source of the acquire imaged or discriminating between authentic images and faked ones. With the development of digital technology and software industry, digital cameras help us acquire high-definition photo easily, and meanwhile the photo can be easily manipulated or the relative information linking between the image and digital camera can be removed, that possibly results into the copyright infringement. Thus, the research of reliable forensic tools remains a hot research topic.

A. STATE OF THE ART

As a consequence, image forensics has received increasing attention from the research community in the past decades. Image forensic techniques can be generally classified into two categories. The first one is defined as active forensics, also referred to as digital watermarking. Since the embedding mechanism has to be available and the credibility of information embedded in the image remains questionable,

the widespread utilization of digital watermarking has been substantially limited. Indeed, watermarking is currently used to prevent movie piracy or to protect authors' copyrights, but almost never for forgery detection. To overcome its drawbacks, another type of forensic methods, defined as passive forensics, has been proposed. Since it does not require to access any prior information on the image, passive forensics has become a more widely adopted method for image authentication.

Forensic techniques can also be classified based on their purpose: image forgery detection and image origin identification (see a complete overview in [1] and [2]). Image forgery detection aims to authenticate any manipulation of a given image such as copy-move, splicing, resampling, contrast enhancing, JPEG compression and median filtering, see [3]–[9] for instance. Image origin identification aims to verify that a given digital image has been captured by a specific camera brand, model or even individual device which is the topic this context mainly focuses on. By investigating the problem of image origin identification,

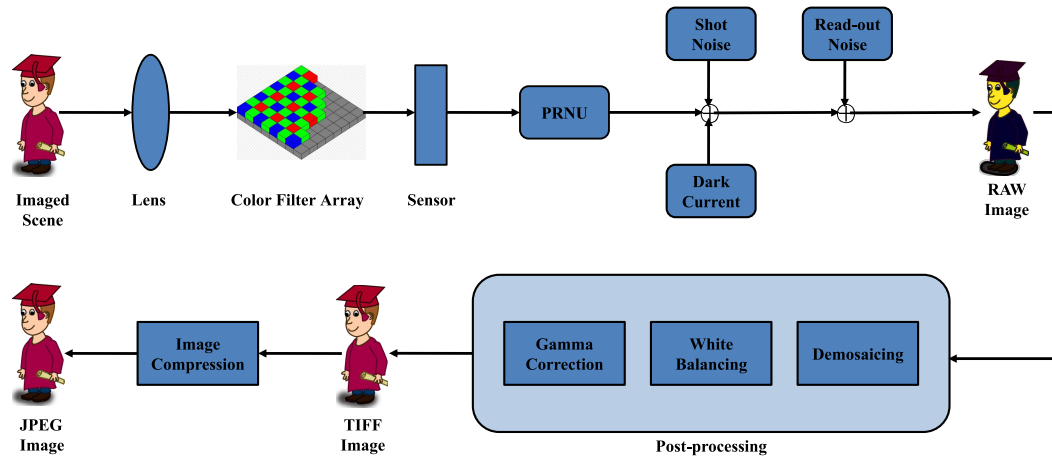


FIGURE 1. Illustration of a typical imaging pipeline within a digital camera.

forensic investigators can link a set of unauthorized images (posted on the web site) to the same camera device whose owner is probably committing some unlawful acts, referring to as user ID identification (see [10]); cameramen can utilize this technique to prevent their pictures from distributing without authorization. In addition, this technique can straightally be extended to the field of image retrieval [11] or clustering [12], [13].

The main idea behind the most forensic algorithms is that the fingerprints can be extracted from image acquisition stages. Hence, it is proposed to generally illustrate a typical imaging pipeline within a digital camera (see Fig. 1). The optical system (e.g. lens) absorbs photons from a scene. Then, the incident light spectrum is filtered by a Color Filter Array (CFA). Relying on an image sensor, the incident lights are converted to an electrical current. Next, an analog-to-digital (A/D) converter embedded within the camera converts the current into digital signal. However, the imaging acquisition pipeline unavoidably leads to additive noises (e.g. shot noise, dark current, read-out noise, etc. ...) and multiplicative noises (Photo-Response Non-Uniformity noise, PRNU for short). Then, following by some post-processing stages (e.g. demosaicing, white balancing, gamma correction), an uncompressed image can be acquired; in this context, this uncompressed high-quality image is referred to as a TIFF (Tagged Image File Format) image. Finally, for storage, an image compression algorithm, such as Joint Photographic Experts Group (JPEG) standard, is applied. A specific overview of the structure and processing stages in a digital still camera is extended in [14] and [15]. In this paper, let us investigate the problem of image origin identification from RAW images.

This paper studies the problem of individual camera device identification using passive method. Hence, let us briefly review the previous works which have the same goal. Passive source camera or image source identification methods, relying on the camera fingerprints left inside the digital image, can generally be categorized into:

- 1) The methods in the first category depend on the image acquisition process. For instance, the algorithm proposed in [16] identified the device origin of a given image in virtue of fingerprints generated from the white balancing. By exploiting the fingerprints extracted from lens aberration, a forensic detector [17] has been proposed for dealing with the problem of identifying the camera model. The challenge of interchangeable-lens cameras to some extent limits the application of the lens aberration-based algorithm. The detectors proposed in [18]–[21] utilized both CFA and demosaicing algorithms to identify the source camera model. Besides, the intrinsic traces caused by JPEG compression (see [22]) were also considered as influential factors for solving the identification problem. These algorithms are generalized under the framework of supervised classification (such as Support Vector Machine, SVM). The challenge is that a few manufacturers share the similar image processing technique, resulting in considerably similar fingerprints. Furthermore, the supervised classification framework, however, unavoidably introduces two main limitations: 1) during its training stage, a large scale of different types of samples (e.g. images) from various sources is required. 2) the statistical performance of the trained classifier is only studied empirically from a testing set, lacking of theoretical analysis. In fact, that is an open problem for all supervised methods [23].
- 2) In the second category, the methodologies exploit the unique noise of each camera model and device as an “intrinsic” fingerprint for source camera identification. During sensor manufacturing process, the inhomogeneity of silicon wafers inevitably results into non-uniformity of photo-electronic conversion (see [14], [24]). Due to the imperfections, Sensor Pattern Noise (SPN) is generated, which was first used for identifying the source camera device [25]. Afterwards, [26]–[29] improved the pioneer algorithm.

Note that the SPN consists of two main components: Fixed Pattern Noise (FPN) and PRNU. The FPN represented by dark current, which was exploited in [30], can be suppressed typically by subtracting a dark frame from the output image. Since the FPN fingerprint is not robust enough, it is not used in later works any more. By contrast, the PRNU performs more robustly. The methods proposed in [26]–[28] and [31] directly studied the algorithms of source camera identification via the PRNU. However, the counter-forensic algorithm [32] challenged the credibility of the SPN-based fingerprint. The main challenge in this category is that the extracted PRNU relies on the image content, which can be severely contaminated by the details of scenes (see [33]). Besides, detectors of the existing literature limitedly investigate the hypothesis theory and statistical image models. Thus, the performance of source camera identification still remains analytically unestablished and is empirically measured on specific databases.

To our knowledge, the algorithms proposed in [25]–[27] have the ability to identify individual camera device, meaning that the detectors can use extracted fingerprints to distinguish the different individual devices, possibly of the same camera model. In this paper, we mainly study the problem of individual camera device identification, which requires more accurate and robust characteristics of the fingerprints. Note that the present paper is an extended version of our prior work [34] and the core contributions of this paper are listed in the next Subsection I-C.

B. MOTIVATION OF THE CONTEXT

With the help of the decrease of data storage costs and the development of photo-editing software, photographers possibly choose to record their picture in a RAW format, instead of a compressed JPEG file. Compared with 8-bit JPEG file in each color channel, for instance, 12 or 14-bit RAW file contains more color information referring to as the more rich dynamic range of pixel intensity. This indeed preserves the very original lossless data captured by the sensor, and allows to manually adjust the post-processing operations to obtain the desired visual results. As a consequence, almost every high-end (such as Digital Single-Lens Reflex, DSLR) still camera, and some economic cameras or even smartphones can let users capture images in a raw format; the forensic research based on RAW format images is thus becoming more and more important.

However, almost all of state-of-the-art forensic detectors are mainly designed for identifying the source camera from JPEG format images. Due to the impact of post-processing and image compression operation, the extracted camera fingerprints from JPEG files become less trustworthy. Besides, the counter-forensic algorithm proposed in [32] maliciously designed the faked camera fingerprints which directly decreased the accuracy of detection. However, a RAW format image provides much more relevant

information¹ which is directly generated by the image sensor and is probably destroyed by post-processing or image compression operation. Thus, a RAW image can be used to perform a more reliable forensic analysis that could be used in court as evidence. Therefore, it makes sense that this paper studies the design of a robust and reliable individual camera device identification method from RAW images.

Our proposed methodology mainly exploits the intrinsic fingerprint of image noise statistical properties to deal with the problem of identifying the individual camera device from RAW images. In virtue of the hypothesis testing theory, we aim to establish the statistical properties of the detector. Additionally, the limitation is that our statistical test can only be applied to identify a source camera from RAW images.

C. CONTRIBUTIONS OF THE PAPER

Let us use the additive noise (e.g. shot noise and read-out noise) as the unique fingerprints for source camera device identification. Although the statistical test proposed in [35] was used for identifying the source camera model, the fingerprints hardly discriminated the individual camera device. Relying on the enhanced Poissonian-Gaussian noise model, it is proposed to design a new statistical detector for identifying the source camera device. Therefore, the main contributions are the following:

- The Poissonian-Gaussian model of [36]–[38] described the pixel distribution, that is all the pixels in a natural RAW image, regardless of their values, share the same model parameters. However, by challenging that assumption, we explicitly describe the statistical properties of pixels as a function of the incident light, or more precisely their expectation, leading to the design of an enhanced Poissonian-Gaussian noise model.
- When all model parameters are known, the Likelihood Ratio Test (LRT) is established and its performance is theoretically analyzed. Meanwhile, the statistical performance of LRT serves as an upper bound on the detection power.
- In a practical context, we design a Generalized Likelihood Ratio Test (GLRT). By using the enhanced Poissonian-Gaussian model, the GLRT can identify, among two different devices, the one with which the inspected image has been captured.
- By combining multiple different GLRTs (serving as sub classifiers), we propose to establish a multi-classifier with the ability of identifying (more than two) camera devices, by which inquiry images are possibly obtained in a close or an open set.
- Numerical simulations verify the sharpness of the theoretically established results. In the practical detection realized over the real data, compared with prior-art methods proposed in [27] and [35], our proposed detector shows its effectiveness.

¹In this context, relevant information refers to as the unique camera fingerprint linking between a RAW format image and its source camera device.

It is also important to acknowledge that the present paper is an extended version of our prior work [34]. This paper extends the results of our prior work [34] in the following directions:

- 1) Enhancing the well-known heteroscedastic Poissonian-Gaussian noise model, we propose a new statistical model in Subsection IIII-B in which parameters (a_k, b_k) (see Equations (7)), that characterize this noise model both depending on a weighting factor w_k (see Fig. 3b). Besides, in this context, we first assume that non-linear relationship between model parameters (a_k, b_k) (see Equation (8)), which is illustrated in Fig. 3b. However, our prior paper only considers the parameters as (a_k, b) .
- 2) In Section III, the proposed optimal LRT is designed considering the parameters (a_k, b_k) and, moreover, the results (see Fig. 5) show that this test outperforms the one proposed in our prior work.
- 3) In Section IV, the proposed practical GLRT also takes into account the parameters (a_k, b_k) and their estimation from images using the weighting factors w_k (see Equations (32) and (33)). Once again, the results obtained with this approach outperform those presented in our prior paper (see Fig. 8).
- 4) In Section V, we design a practical multi-classifier dealing with the scenario of identifying multiple camera devices.
- 5) Last, but not least, this paper provides a wide range of experiments to confirm the efficiency of the proposed method and includes comparison with state-of-the-art approaches.

D. ORGANIZATION OF THE PAPER

The rest of this paper is organized as follows. After reviewing the Poissonian-Gaussian noise model, Section II proposes the enhanced version of the model for a RAW image. In Section III, relying on the enhanced Poissonian-Gaussian noise model, an optimal LRT is given with assuming that the statistical properties of each pixel is perfectly known. In this ideal scenario, the statistical performance of this LRT is established, serving as an upper bound on individual device identification. Then, Section IV presents a practical GLRT with the estimation of the expectation of each pixel. Furthermore, it is proposed to design a multi-classifier in Section V. Then, Section VI presents numerical results of the proposed detectors on the simulated and real images. Finally, Section VII concludes this paper.

II. PROPOSED CAMERA FINGERPRINTS FOR RAW IMAGES

A. OVERVIEW ON POISSONIAN-GAUSSIAN NOISE MODEL AND ITS LIMITATION

We assume that a vector $\mathbf{Z} = \{z_i\}$ of I pixels where $i \in \{1, \dots, I\}$, denotes a natural RAW image. The photo-electron conversion essentially consists in a counting process, which can be modeled as a Poisson process. Then, the number of the collected electrons, denoted as N_{e_i} , includes two main

portions: the sum of the electrons generated by the incident photons N_{p_i} and the dark electrons N_{t_i} generated by thermal noise. Then N_{e_i} is defined by:

$$N_{e_i} \sim \mathcal{P}(\eta_i N_{p_i} + N_{t_i}), \quad (1)$$

where $\mathcal{P}(\cdot)$ represents the Poisson distribution; η_i denotes a conversion factor with accounting for filter transmittance and quantum efficiency. By using Poissonian-Gaussian noise model, we do not consider the impact of PRNU or FPN. Thus, for each pixel, the photosensitivity and thermal noise are constant; it is proposed to omit the index i from η and N_t . In the process of read-out, different sources of electronic noise, modeled as a zero-mean Gaussian random variable ϵ_i with variance ω^2 , possibly corrupt the recorded signal. Note that read-out noise, which is stationary and independent of the signal, does not change among different images. Then z_i can be described by:

$$z_i = g \cdot (N_{e_i} + \epsilon_i), \quad (2)$$

where g represents the analog gain controlled by International Standardization Organization (ISO) sensitivity setting. RAW pixels are statistically independent (see details in [36] and [38]). Since the number of electrons for each pixel is large enough, it is proposed to utilize the Gaussian approximation of the Poisson distribution. Then we can acquire the following definition:

$$z_i \sim \mathcal{N}(\mu_i, a\mu_i + b), \quad (3)$$

where the Gaussian distribution is denoted as $\mathcal{N}(\cdot)$ with the pixel expectation $\mu_i = g \cdot (\eta N_{p_i} + N_t)$; its variance $v_i = a\mu_i + b$. The parameters (a, b) can respectively be described by:

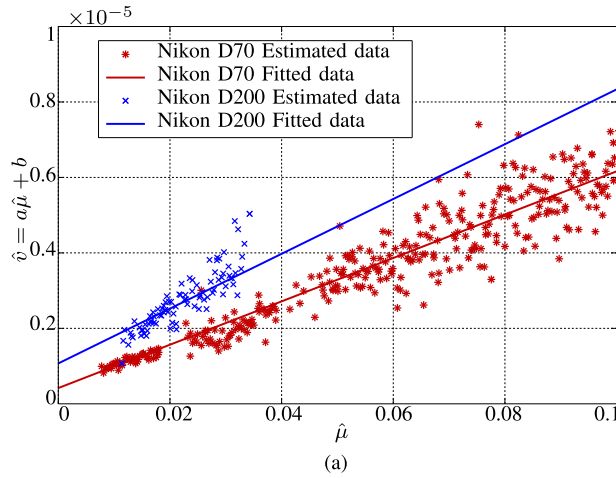
$$a = g \quad \text{and} \quad b = g^2 \omega^2. \quad (4)$$

In some digital imaging sensors, the collected electrons N_{e_i} is compensated by a base pedestal parameter p_0 , leading to an offset-from-zero of the output pixel, which can be represented by:

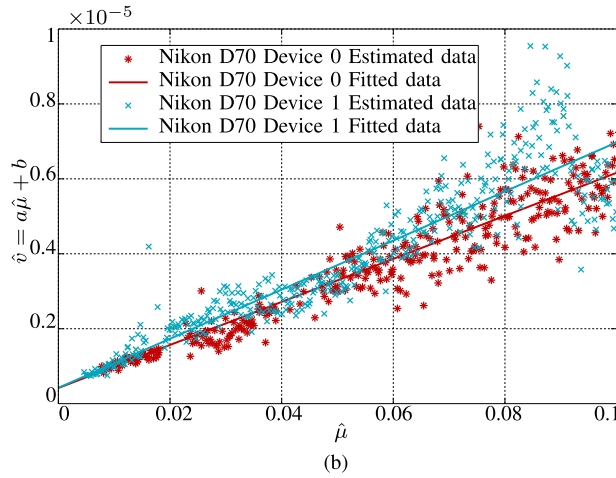
$$z_i = g \cdot [p_0 + \mathcal{P}(\eta_i N_{p_i} + N_{t_i} - p_0) + \mathcal{N}(0, \omega^2)], \quad (5)$$

where $a = g$ and $b = g^2(\omega^2 - p_0)$ (see details in [36]). It is thus straightforward that in the case of $p_0 > \omega^2$, one has $b < 0$. For simplicity, (a, b) is defined as the camera parameters and the pixel expected value μ_i as the image parameter.

The ISO sensitivity g mainly controls the camera parameters (a, b) . Besides, other camera settings such as focal length, shutter speed, and integration time might more or less impact the parameters (a, b) , which can be ignored in this context. Therefore, for a RAW format image, the problem of source camera identification has to be studied with the constant ISO value while it allows the changes of other camera settings. The parameter a is proportional to ISO sensitivity; the parameter b is proportional to its square. Furthermore, when assuming that ISO sensitivity g is acquired before an image is generated from a digital device, we can predict a



(a)



(b)

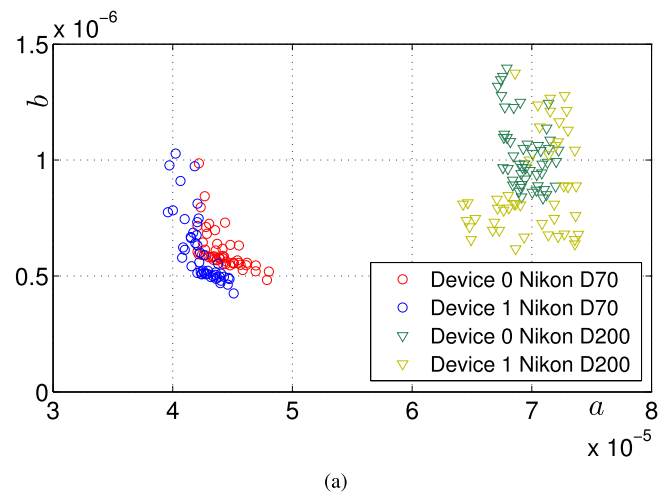
FIGURE 2. Illustration of Scatter-plot of pixels' expectation $\hat{\mu}$ and variance \hat{v} , which can be respectively estimated using Equations (27) and (28). (a) Results from RAW images of Nikon D200 and Nikon D70. (b) Results from RAW images of Nikon D70 Device 0 and Nikon D70 Device 1.

linear relationship between pixels' expectation and variance referring to Equation (3), which is illustrated in Fig. 2a.

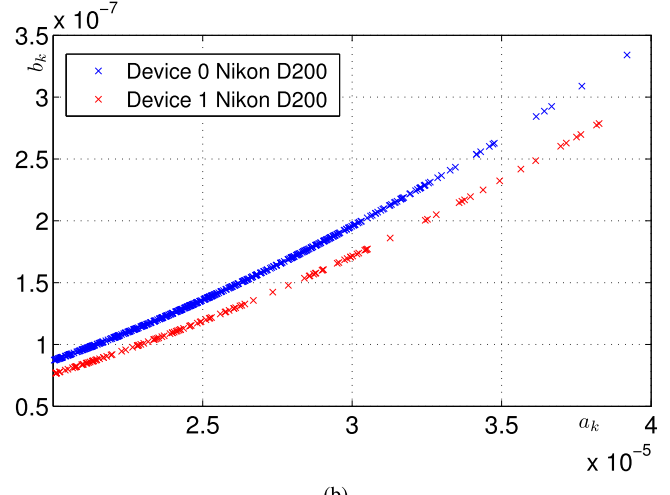
However, due to the spatial variation in the pixel response, e.g. PRNU, the camera parameters (a, b) probably do not remain constant for all the pixels. In addition, via the noise model (3), we cannot deal with the problem of identifying the individual camera device. Fig. 2b illustrates the linear relationship from different devices of the same camera model. Most overlapped portions of the estimated data imply that the constant camera parameters (a, b) from two devices of *Nikon D70/D200* cannot be distinguished (see Fig. 3a). Hence, by taking into account pixels' response non-uniformity, we improve this Poissonian-Gaussian noise model in order to identify the individual device in the following subsection.

B. NOISE MODEL IMPROVEMENT

In the relation (4), the parameter g might not be constant in practice due to the variation in the pixel response, e.g. PRNU. The heteroscedastic noise model (3) characterizes



(a)



(b)

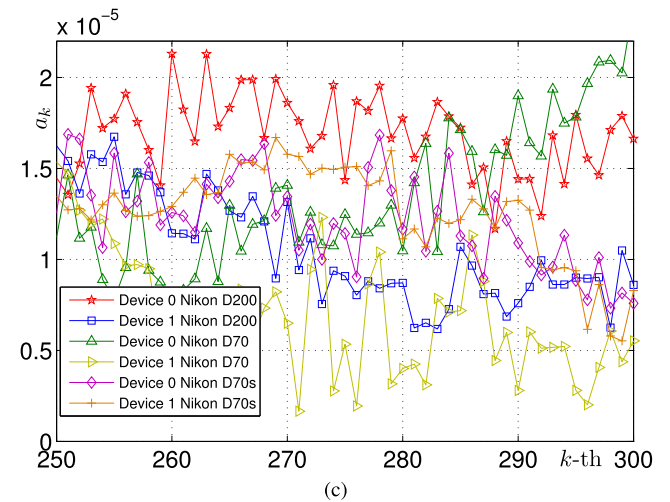


FIGURE 3. Camera fingerprints comparison of different devices per camera model with ISO 200. Natural RAW images for Nikon D70, Nikon D70s and Nikon D200 are from the Dresden image database [39]. (a) Camera parameters (a, b) estimated using [35] from 50 RAW images. (b) Camera parameters (a_k, b_k) proposed of k -th level set where the non-linear relationship is expressed by $b_k = \frac{b}{a^2} a_k^2$. (c) Camera parameter a_k in k -th level set. For simplicity, only a part of level sets are selected for comparison.

the response of a digital imaging sensor. This noise model accounts for the noises corrupting the RAW image at the sensor output. Moreover, this noise model supposes a constant response for a number of electrons counted for each pixel, e.g. g constant. In fact, the sensor response characterized by this coefficient is not constant and is slightly different for two instances of the same camera model.

Then, it is proposed to define the fingerprints of the camera source device as (\mathbf{a}, \mathbf{b}) , in which the vector $\mathbf{a} = \{a_1, \dots, a_K\}$, $\mathbf{b} = \{b_1, \dots, b_K\}$ represent the parameters used for linking between all the expectation and variance value of the pixel intensity; $k \in \{1, \dots, K\}$ denotes an index for each level set, with K the number of level sets. Here, level actually represents that the specific position among the whole dynamic range of intensity where the pixel value falls; all the pixels falling in the same level consist of a level set. Each level set is characterized by its center value u_i and allowed deviation Δ defining the dynamic range of each level, $\mu_i \in [u_i - \frac{\Delta}{2}, u_i + \frac{\Delta}{2}]$. In practice, assuming a signal in the range $[0, 1]$, one can take fixed $\Delta_i \equiv \Delta$ and evenly spaced $u_i \in \{\Delta_j, j = 1, \dots, K = \lfloor \Delta^{-1} \rfloor\}$, where the $\lfloor \cdot \rfloor$ indicates the rounding to the nearest larger or equal integer. Thus, the following accurate noise model is defined as:

$$z_i \sim \mathcal{N}(\mu_i, a_k \mu_i + b_k), \quad (6)$$

$$\text{with } a_k = a \cdot w_k, b_k = b \cdot w_k^2, \quad (7)$$

where $\mathcal{N}(\cdot)$ denotes the Gaussian distribution with the expectation μ_i and variance $a_k \mu_i + b_k$. The camera parameters (a_k, b_k) represent the unique fingerprints from the k -th level set. Let us formulate the non-linear relationship between a_k and b_k in the k -th level set by:

$$b_k = \frac{b}{a^2} a_k^2. \quad (8)$$

It is proposed to illustrate the relationship in Fig. 3b. Note that when $w_k = 1$, the proposed enhanced Poissonian-Gaussian model (6) is regressed back to the noise model (3).

It is proposed to compare our estimated camera fingerprints based on the model (6) with the fingerprints based on the model (3) proposed in [35]. As Fig. 3a illustrates, the camera fingerprints (a, b) can be used to distinguish between *Nikon D70* and *Nikon D200*, but are invalid for different devices of the same camera model. By contrast, Fig. 3b and 3c both illustrate that the fingerprints (a_k, b_k) proposed in this paper are very discriminative when identifying different devices of the same model. Then, in Section III, based on our proposed enhanced noise model, we design the LRT with knowing all model parameters, and to establish its statistical properties. In a practical scenario, in Section IV, let us establish the GLRT, which can identify among two camera devices the one capturing the image under investigation.

III. INDIVIDUAL CAMERA DEVICE IDENTIFICATION: OPTIMAL LIKELIHOOD RATIO TEST

This paper proposes to use the enhanced Poissonian-Gaussian statistical model of the noise (6) to address the problem of

individual camera device identification. Indeed, as shown in the previous Section II, the parameters of this model change significantly from two different camera devices, even though those cameras are from the same model. Hence, let us formally state the problem of individual camera device identification based on the parameters of the enhanced Poissonian-Gaussian statistical model of the noise; then, the optimal LR test is studied and its statistical performance is theoretically established.

It is proposed to define an inspected image \mathbf{Z} , and two camera sources \mathcal{S}_0 and \mathcal{S}_1 , referring to as individual devices, are required to be identified. Then, let us cast the problem of source camera identification into the following framework. In this scenario, a forensic investigator chooses between the following bi-criteria hypotheses:

$$\begin{cases} \mathcal{H}_0 : \mathbf{Z} \text{ acquired by camera source } \mathcal{S}_0 \\ \mathcal{H}_1 : \mathbf{Z} \text{ acquired by camera source } \mathcal{S}_1 \text{ different from } \mathcal{S}_0. \end{cases}$$

A. STATEMENT OF THE PROBLEM

We assume that the natural RAW image under investigation $\mathbf{Z} = \{z_i\}$ has been captured either by source camera \mathcal{S}_0 or by source camera \mathcal{S}_1 . In addition, it is also assumed that for each camera device $\mathcal{S}_j, j \in \{0, 1\}$, the noise model parameters $(a_{k,j}, b_{k,j})$ are perfectly known. In fact, in an operational context, the number of images captured with each device is sufficiently large to ensure an accurate estimation of those parameters. The problem of camera device identification essentially consists of choosing between the two following hypotheses \mathcal{H}_0 : “*the pixels z_i follow the Gaussian distribution $\mathcal{N}(\mu_i, a_{k,0}\mu_i + b_{k,0})$* ” and \mathcal{H}_1 : “*the pixels z_i follow the Gaussian distribution $\mathcal{N}(\mu_i, a_{k,1}\mu_i + b_{k,1})$* ” which can be written as:

$$\begin{cases} \mathcal{H}_0 : \{z_i \sim \mathcal{N}(\mu_i, a_{k,0}\mu_i + b_{k,0})\}, \\ \mathcal{H}_1 : \{z_i \sim \mathcal{N}(\mu_i, a_{k,1}\mu_i + b_{k,1})\}. \end{cases} \quad (9)$$

Formally, a statistical test is a mapping $\delta : \mathbb{Z}^{I,J} \mapsto \{\mathcal{H}_0, \mathcal{H}_1\}$ such that hypothesis \mathcal{H}_j is accepted if $\delta(\mathbf{Z}) = \mathcal{H}_j$ (see [40] for a complete introduction). As previously explained, this paper aims at providing a reliable test; hence, this paper focuses on the Neyman-Pearson bi-criteria approach which aims at maximizing the correct detection probability for a given false alarm probability α_0 . For the sake of clarity, let us define the false alarm probability as:

$$\alpha_0 = \mathbb{P}_{\mathcal{H}_0}[\delta(\mathbf{Z}) = \mathcal{H}_1], \quad (10)$$

where $\mathbb{P}_{\mathcal{H}_i}[E]$ stands for the conditional probability of the event E under the hypothesis $\mathcal{H}_j, j \in \{0, 1\}$. In the framework of Neyman-Pearson it is also important to define the class of tests with a false alarm probability upper-bounded by α_0 as follows:

$$\mathcal{K}_{\alpha_0} = \left\{ \delta : \sup_{\theta_0} \mathbb{P}_{\mathcal{H}_0}[\delta(\mathbf{Z}) = \mathcal{H}_1] \leq \alpha_0 \right\}. \quad (11)$$

Here the supremum over model parameters θ_0 , in which $\theta_0 = (a_{k,0}, b_{k,0}, \mu_i)$, ensures that the false alarm probability α_0

cannot be exceeded whatever the distribution parameters might be. Among all the tests in the class \mathcal{K}_{α_0} , it is aimed at finding a test δ which maximizes the power function, often referred to as the probability of correct detection or true positive rate:

$$\beta_\delta = \mathbb{P}_{\mathcal{H}_1}[\delta(\mathbf{Z}) = \mathcal{H}_1], \quad (12)$$

which is equivalent to minimizing the false negative probability $\alpha_1(\delta) = \mathbb{P}_{\mathcal{H}_1}[\delta(\mathbf{Z}) = \mathcal{H}_0] = 1 - \beta_\delta$.

Though several assumptions have been mentioned, the statement of the problem as formulated in Equation (9) highlights the main difficulties of using image noise model for individual camera device identification. First, the optimal test which achieves the highest detection power is not known (it has been studied in our prior work [34]). Such a result would indeed provide an important upper bound on the performance one can expect for distinguishing individual camera devices. Second, in a practical context, neither the camera device parameters $(a_{k,j}, b_{k,j})$, where $k \in \{1, \dots, K\}$ and $j \in \{0, 1\}$, nor the image parameter μ_i , where $i \in \{1, \dots, I\}$, are known. Obviously, those parameters play a different role. Indeed, the expectation of pixels μ_i are nuisance parameters, as they do not have any interest to solve the detection problem of device identification (9), but they must be carefully taken into account. On the other hand, the camera device parameters $(a_{k,j}, b_{k,j})$ have to be estimated from the inspected image. In such a case the first problem consists in estimating those camera parameters, and the second problem is that the statistical hypotheses become composite. In such a case an optimal statistical test seldom exists.

In the following subsections, we will present the optimal LRT and establish analytically its statistical performance. To deal with the practical, yet more complicated, case in which the nuisance parameters, that is the pixel expectation μ_i , are unknown, a practical statistical test will be presented in Section IV.

B. OPTIMAL DETECTION FRAMEWORK

In the ideal settings where the image parameters are known, the problem (9) can be solved by designing a statistical test between two simple hypotheses. In this scenario, it is well known from the Neyman-Pearson Lemma [40, Th. 3.2.1] that the most powerful test in the class \mathcal{K}_{α_0} (11) is the LRT defined, assuming that pixels z_i are independent, as:

$$\delta^{\text{lr}}(\mathbf{Z}) = \begin{cases} \mathcal{H}_0 & \text{if } \Lambda^{\text{lr}}(\mathbf{Z}) = \sum_{i=1}^I \Lambda^{\text{lr}}(z_i) < \tau^{\text{lr}}, \\ \mathcal{H}_1 & \text{if } \Lambda^{\text{lr}}(\mathbf{Z}) = \sum_{i=1}^I \Lambda^{\text{lr}}(z_i) \geq \tau^{\text{lr}}, \end{cases} \quad (13)$$

where the decision threshold τ^{lr} is the solution of the Equation $\mathbb{P}_{\mathcal{H}_0}[\Lambda^{\text{lr}}(\mathbf{Z}) \geq \tau^{\text{lr}}] = \alpha_0$, to guarantee that the false alarm probability of the LRT equals α_0 . Let us denote \mathcal{P}_{θ_0} and \mathcal{P}_{θ_1} the probability density function (pdf) of the observations z_i under each observation under hypothesis \mathcal{H}_0 and \mathcal{H}_1 ;

here θ_j , $j = \{0, 1\}$ represents the vector $(a_{k,j}, b_{k,j}, \mu_i)$ of distribution parameters. Based on the heteroscedastic Gaussian model proposed in this paper (9), the log Likelihood Ratio (LR)² for one observation is given by:

$$\Lambda^{\text{lr}}(z_i) = \log \frac{\mathcal{P}_{\theta_1}[z_i]}{\mathcal{P}_{\theta_0}[z_i]}. \quad (14)$$

From the definition of (9), it is straightforward to demonstrate that the LR (14) is given by:

$$\Lambda^{\text{lr}}(z_i) = \log \left(\frac{\sigma_{i,0}}{\sigma_{i,1}} \right) + \frac{\sigma_{i,1}^2 - \sigma_{i,0}^2}{2\sigma_{i,1}^2 \sigma_{i,0}^2} (z_i - \mu_i)^2, \quad (15)$$

where the variance $\sigma_{i,j}^2 = a_{k,j}\mu_i + b_{k,j}$, $j \in \{0, 1\}$ and level set index $k \in \{1, \dots, K\}$.

C. THEORETICAL STATISTICAL PERFORMANCE OF THE OPTIMAL LRT

Again, since the observations z_i are statistically independent random variables (though their expectations are close they are not correlated), the LR $\Lambda^{\text{lr}}(\mathbf{Z})$ can be simply given, meaning that when the number of pixels becomes “sufficiently large”, the sum of random variables and some asymptotic theorems allow us to establish its distribution. Let us denote $E_{\mathcal{H}_j}(\Lambda^{\text{lr}}(z_i))$ and $V_{\mathcal{H}_j}(\Lambda^{\text{lr}}(z_i))$ the expectation and the variance, respectively, of the LR $\Lambda^{\text{lr}}(z_i)$ under hypothesis \mathcal{H}_j , $j = \{0, 1\}$. In order to study the asymptotic properties of the proposed test, let us recall that the Lindeberg-Feller central limit theorem (CLT) [40, Th. 11.2.5] that when the number of pixels I tends to infinity, it holds true that³:

$$\frac{\sum_{i=1}^I \Lambda^{\text{lr}}(z_i) - E_{\mathcal{H}_j}(\Lambda^{\text{lr}}(z_i))}{\left(\sum_{i=1}^I V_{\mathcal{H}_j}(\Lambda^{\text{lr}}(z_i)) \right)^{1/2}} \xrightarrow{d} \mathcal{N}(0, 1), \quad j \in \{0, 1\}, \quad (16)$$

where \xrightarrow{d} represents the convergence in distribution. This theorem (16) is of crucial interest to establish the asymptotic statistical properties of the proposed test [41]–[46] as indeed one can use the moments of the LR $\Lambda^{\text{lr}}(\mathbf{z}_i)$ under \mathcal{H}_0 to normalize $\Lambda^{\text{lr}}(\mathbf{Z})$, see Equation (13), as follows:

$$\bar{\Lambda}^{\text{lr}}(\mathbf{Z}) = \frac{\Lambda^{\text{lr}}(\mathbf{Z}) - \sum_{i=1}^I E_{\mathcal{H}_0}(\Lambda^{\text{lr}}(z_i))}{\left(\sum_{i=1}^I V_{\mathcal{H}_0}(\Lambda^{\text{lr}}(z_i)) \right)^{1/2}}. \quad (17)$$

It is thus straightforward to define consequently the normalized decision function based on the LR $\bar{\Lambda}^{\text{lr}}(\mathbf{Z})$ as follows:

$$\bar{\delta}^{\text{lr}}(\mathbf{Z}) = \begin{cases} \mathcal{H}_0 & \text{if } \bar{\Lambda}^{\text{lr}}(\mathbf{Z}) < \bar{\tau}^{\text{lr}} \\ \mathcal{H}_1 & \text{if } \bar{\Lambda}^{\text{lr}}(\mathbf{Z}) \geq \bar{\tau}^{\text{lr}} \end{cases} \quad (18)$$

²For simplicity in this paper, the term LR refers to the log value of likelihood ratio.

³Note that we refer to the Lindeberg-Feller CLT, whose conditions are easily verified in our case, because the random variables are independent but are not identically distributed.

For simplicity, it is proposed to denote

$$m_j = \sum_{i=1}^I E_{\mathcal{H}_j}(\Lambda^{\text{lr}}(z_i)), \quad (19)$$

$$\sigma_j^2 = \sum_{i=1}^I V_{\mathcal{H}_j}(\Lambda^{\text{lr}}(z_i)), \quad (20)$$

the expectation and variance of the LR $\Lambda^{\text{lr}}(\mathbf{Z})$, with, of course $j \in \{0, 1\}$. Some algebra show that for each observation z_i the expectation and the variance of the LR $\Lambda^{\text{lr}}(z_i)$ are given by:

$$E_{\mathcal{H}_j}(\Lambda^{\text{lr}}(z_i)) = \frac{1}{2} \log \frac{a_{k,0}\mu_i + b_{k,0}}{a_{k,1}\mu_i + b_{k,1}} + \frac{1}{2} \left(\frac{\sigma_{i,j}^2}{a_{k,0}\mu_i + b_{k,0}} - \frac{\sigma_{i,j}^2}{a_{k,1}\mu_i + b_{k,1}} \right) \quad (21)$$

$$V_{\mathcal{H}_j}(\Lambda^{\text{lr}}(z_i)) = \frac{\sigma_{i,j}^4}{2} \left(\frac{1}{a_{k,0}\mu_i + b_{k,0}} - \frac{1}{a_{k,1}\mu_i + b_{k,1}} \right)^2. \quad (22)$$

Then it is straightforward to establish the statistical properties of the proposed test (18), involving the decision threshold $\bar{\tau}^{\text{lr}}$ and the detection power $\beta_{\delta^{\text{lr}}}$, which are given in the following propositions. For clarity, Φ and Φ^{-1} respectively represent the cumulative distribution function (cdf) of the standard normal distribution and its inverse.

Proposition 1: On the assumption that both the camera parameters $(a_{k,j}, b_{k,j})$ and the image parameters μ_i are known, then for any $\alpha_0 \in (0, 1)$ the camera model identification as stated in (9) can be solved using the decision threshold:

$$\bar{\tau}^{\text{lr}} = \Phi^{-1}(1 - \alpha_0), \quad (23)$$

which guarantees that test $\bar{\delta}^{\text{lr}}(\mathbf{Z})$ (18) is in the class \mathcal{K}_{α_0} .

Proposition 2: Under the same condition as stated in Proposition 1, then for any decision threshold $\bar{\tau}^{\text{lr}}$, the power function associated with the proposed test $\bar{\delta}^{\text{lr}}(\mathbf{Z})$ (18) is given by:

$$\beta_{\delta^{\text{lr}}} = 1 - \Phi \left(\frac{\sigma_0}{\sigma_1} \cdot \bar{\tau}^{\text{lr}} + \frac{m_0 - m_1}{\sigma_1} \right). \quad (24)$$

The main advantages of normalizing the LR as described in the relation (17) are emphasized: it allows us to set any threshold with ensuring a false alarm probability independently of any distribution parameter. Additionally, when identifying the source camera device, the detection power $\beta_{\delta^{\text{lr}}}$ can serve as an upper limit for any statistical detector.

However, it is not practical that both camera parameters $(a_{k,j}, b_{k,j})$ of two individual devices and image parameters μ_i are perfectly known. Thus, in the next Section IV, let us design the test to deal with unknown camera and image parameters. The problem, thus, becomes to estimate, from the inspected image \mathbf{Z} , the expectation of pixels and uses those to estimate the camera parameters and finally to investigate the statistical properties of the GLRT.

IV. DEALING WITH UNKNOWN PARAMETERS: GENERALIZED LIKELIHOOD RATIO TEST WITH ESTIMATED CAMERA PARAMETERS

A. CAMERA PARAMETERS ESTIMATION

In the present paper, we use the segmentation algorithm proposed in [36] to deal with unknown camera parameters and to estimate the heteroscedastic Gaussian noise model parameters. The generalization of the proposed method is the following: first, the image \mathbf{Z} is transformed into the wavelet domain in order to estimate the expectation of all the pixels. Then, let us partition the range of the normalized estimation of pixels' expectation (e.g., $[0, 1]$) into K sub-ranges. Note that image \mathbf{Z} is segmented into K non-overlapping “homogeneous level sets” (that is pixels with close estimated expectations), denoted S_k , of size n_k , $k \in \{1, \dots, K\}$. Since the pixels can accurately be modeled as statistically independent, we assume that within each level set S_k , all the pixels are realization of i.i.d. random variable. Due to the proposed enhanced Poissonian-Gaussian noise model (6), it is reasonable that all the pixels with the same expectation share the same variance. Then, it is proposed to denote $\mathbf{z}_k^{\text{wapp}} = \{z_{k,i}^{\text{wapp}}\}_{i=1}^{n_k}$ and $\mathbf{z}_k^{\text{wdet}} = \{z_{k,i}^{\text{wdet}}\}_{i=1}^{n_k}$ as the vector of wavelet approximation coefficients and detail coefficients respectively. Due to the linear property of the wavelet transformation, we can apply the proposed noise model in the spatial domain to the wavelet domain (see details in [36]). Let us thus immediately establish the Gaussian distribution followed by the coefficients $z_{k,i}^{\text{wapp}}$ and $z_{k,i}^{\text{wdet}}$

$$z_{k,i}^{\text{wapp}} \sim \mathcal{N}(\mu_k, \|\phi\|_2^2 \sigma_k^2) \quad (25)$$

$$z_{k,i}^{\text{wdet}} \sim \mathcal{N}(0, \sigma_k^2) \quad (26)$$

where the linear relationship between the expectation and variance is denoted as $\sigma_k^2 = a_k \mu_k + b_k$; ϕ denotes the 2D normalized wavelet scaling function. Then, in k -th level set, the Maximum Likelihood (ML) estimations of the local pixels' expectation:

$$\hat{\mu}_k = \frac{1}{n_k} \sum_{i=1}^{n_k} z_{k,i}^{\text{wapp}}, \quad (27)$$

and of the local pixels' variance:

$$\hat{\nu}_k = \frac{1}{n_k - 1} \sum_{i=1}^{n_k} (z_{k,i}^{\text{wdet}} - \frac{1}{n_k} \sum_{i=1}^{n_k} z_{k,i}^{\text{wdet}})^2 \quad (28)$$

can be averaged over several images by:

$$\hat{\mu}_k^* = \frac{1}{N \cdot n_k} \sum_{n=1}^N \sum_{i=1}^{n_k} z_{k,i}^{\text{wapp}} \quad (29)$$

$$\hat{\nu}_k^* = \frac{1}{N \cdot (n_k - 1)} \sum_{n=1}^N \sum_{i=1}^{n_k} (z_{k,i}^{\text{wdet}} - \frac{1}{n_k} \sum_{i=1}^{n_k} z_{k,i}^{\text{wdet}})^2 \quad (30)$$

in which the vector $n \in \{1, \dots, N\}$ represents the index of images used to average the estimations. Then we estimate the parameters (\hat{a}, \hat{b}) , describing the overall relation between pixels' expectation and variance, see Equation (3), using the

weighted least square approach as proposed in [35]; then, using the linear relationship between expectation $\hat{\mu}_k^*$ and variance \hat{v}_k^* (6), the quadratic equation, linking between the estimated variance \hat{v}_k^* and the variance, is formulated by:

$$\hat{v}_k^* = \hat{\mu}_k^* \cdot \hat{a}_k + \frac{\hat{b}}{\hat{a}^2} \cdot \hat{a}_k^2. \quad (31)$$

Let us use the solution of Equation (31) as a fast and accurate estimation of camera parameters a_k as follows:

$$\hat{a}_k = \frac{\hat{a}^2 \sqrt{\hat{\mu}_k^{*2} + \frac{4\hat{v}_k^*\hat{b}}{\hat{a}^2}} - \hat{a}^2 \cdot \hat{\mu}_k^*}{2\hat{b}}. \quad (32)$$

Relying on the non-linear relationship between b_k and a_k (8), it follows that from the estimations a_k , the parameters b_k can be estimated by:

$$\hat{b}_k = \hat{b} \cdot w_k^2 \quad (33)$$

where the weighting vector is given by $w_k = \frac{\hat{a}_k}{\hat{a}}$.

B. DESIGN OF THE PRACTICAL GLRT

On the assumption that all the model parameters are known for each pixel, we have given the general framework of the hypothesis testing theory. In the practical identification, it is proposed to assume that only the camera parameters $(a_{k,0}, b_{k,0})$ and $(a_{k,1}, b_{k,1})$ are known, while image parameter μ_k are unknown. In this scenario, the practical test intends to identify the inspected image \mathbf{Z} acquired either by device S_0 or device S_1 . Let us adopt a usual solution, which consists in replacing the unknown parameter by its ML estimation. This directly results into the establishment of the following practical GLRT:

$$\hat{\delta}_1(\mathbf{Z}) = \begin{cases} \mathcal{H}_0 & \text{if } \hat{\Lambda}_1(\mathbf{Z}) = \sum_{k=1}^K \sum_{i=1}^{n_k} \hat{\Lambda}_1(z_{k,i}^{\text{wapp}}) < \hat{\tau}_1, \\ \mathcal{H}_1 & \text{if } \hat{\Lambda}_1(\mathbf{Z}) = \sum_{k=1}^K \sum_{i=1}^{n_k} \hat{\Lambda}_1(z_{k,i}^{\text{wapp}}) \geq \hat{\tau}_1, \end{cases} \quad (34)$$

where $\hat{\tau}_1$ represents the solution of equation:

$$\mathbb{P}_{\mathcal{H}_0}[\hat{\Lambda}_1(\mathbf{Z}) \geq \hat{\tau}_1] = \alpha_0, \quad (35)$$

and the log Generalized Likelihood Ratio (GLR)⁴, denoted $\hat{\Lambda}_1(z_{k,i}^{\text{wapp}})$ which is given, for each pixel, by:

$$\begin{aligned} \hat{\Lambda}_1(z_{k,i}^{\text{wapp}}) = & \frac{1}{2} \log \frac{a_{k,0}\hat{\mu}_k + b_{k,0}}{a_{k,1}\hat{\mu}_k + b_{k,1}}, \\ & + \frac{1}{2} \left(\frac{1}{a_{k,0}\hat{\mu}_k + b_{k,0}} - \frac{1}{a_{k,1}\hat{\mu}_k + b_{k,1}} \right) \\ & \cdot \frac{(z_{k,i}^{\text{wapp}} - \hat{\mu}_k)^2}{\|\phi\|_2^2}, \end{aligned} \quad (36)$$

where $\hat{\mu}_k$ denotes the estimated value of pixels' expectation from the k -th level set, as given in Equation (27). Then we

⁴For simplicity in this paper, the term GLR refers to the log value of generalized likelihood ratio.

propose to obtain a normalized GLR $\hat{\Lambda}_2(\mathbf{Z})$ for the entire image with redefining Equation (36) as:

$$\hat{\Lambda}_2(\mathbf{Z}) = \frac{\sum_{k=1}^K \sum_{i=1}^{n_k} \hat{\Lambda}_1(z_{k,i}^{\text{wapp}}) - E_{\mathcal{H}_0}(\hat{\Lambda}_1)}{\left(\sum_{k=1}^K \sum_{i=1}^{n_k} V_{\mathcal{H}_0}(\hat{\Lambda}_1) \right)^{1/2}}. \quad (37)$$

Hence, the corresponding normalized GLRT is formulated by:

$$\hat{\delta}_2(\mathbf{Z}) = \begin{cases} \mathcal{H}_0 & \text{if } \hat{\Lambda}_2(\mathbf{Z}) < \hat{\tau}_2, \\ \mathcal{H}_1 & \text{if } \hat{\Lambda}_2(\mathbf{Z}) \geq \hat{\tau}_2. \end{cases} \quad (38)$$

For simplicity, let us denote

$$m'_j = \sum_{k=1}^K \sum_{i=1}^{n_k} E_{\mathcal{H}_j}(\hat{\Lambda}_1(z_{k,i}^{\text{wapp}})), \quad (39)$$

$$o_j'^2 = \sum_{k=1}^K \sum_{i=1}^{n_k} V_{\mathcal{H}_j}(\hat{\Lambda}_1(z_{k,i}^{\text{wapp}})), \quad (40)$$

as the expectation and variance for GLR $\hat{\Lambda}_1(\mathbf{Z})$ in which $j \in \{0, 1\}$. Immediately, the expectation and variance for each GLR $\hat{\Lambda}_1(z_{k,i}^{\text{wapp}})$ can be expressed by:

$$\begin{aligned} E_{\mathcal{H}_j}(\hat{\Lambda}_1) = & \frac{1}{2} \log \frac{a_{k,0}\mu_k + b_{k,0}}{a_{k,1}\mu_k + b_{k,1}} \\ & + \frac{1}{2} \left(\frac{1}{a_{k,0}\mu_k + b_{k,0}} - \frac{1}{a_{k,1}\mu_k + b_{k,1}} \right) \\ & \cdot (\sigma_{k,j}^2 + \frac{\sigma_{k,j}^2}{n_k}), \end{aligned} \quad (41)$$

$$\begin{aligned} V_{\mathcal{H}_j}(\hat{\Lambda}_1) = & \frac{\sigma_{k,j}^2 \|\phi\|_2^2}{4n_k} \left(\frac{a_{k,0}b_{k,1} - a_{k,1}b_{k,0}}{(a_{k,0}\mu_k + b_{k,0})(a_{k,1}\mu_k + b_{k,1})} \right)^2 \\ & + \frac{\sigma_{k,j}^4}{2} \left(\frac{1}{a_{k,0}\mu_k + b_{k,0}} - \frac{1}{a_{k,1}\mu_k + b_{k,1}} \right)^2 (1 + \frac{1}{n_k})^2 \\ & + \frac{3\|\phi\|_2^2\sigma_{k,j}^6}{4n_k} \left(\frac{a_{k,1}}{(a_{k,1}\mu_k + b_{k,1})^2} - \frac{a_{k,0}}{(a_{k,0}\mu_k + b_{k,0})^2} \right)^2 \\ & \cdot (1 + \frac{1}{n_k})^2, \end{aligned} \quad (42)$$

where in our proposed GLRT, since the image parameter μ_k is unknown, we replace μ_k with $\hat{\mu}_k$. The readers can refer to [35, Appendix B] for the mathematical deduction of $E_{\mathcal{H}_j}(\hat{\Lambda}_1)$ and $V_{\mathcal{H}_j}(\hat{\Lambda}_1)$.

Without the loss of generality, in the following two propositions, one can provide the statistical properties of the proposed GLRT with analytically expressing the decision threshold $\hat{\tau}_2$ for a prescribed false alarm probability and the detection power $\beta_{\hat{\delta}_2}$.

Proposition 3: On the assumption that the pixels are modeled by the proposed enhanced Poissonian-Gaussian model (6), when the camera parameters $(a_{k,j}, b_{k,j})$ are known and the pixels' expectations $\hat{\mu}_k$ are estimated as in (27),

then any $\alpha_0 \in (0, 1)$ the decision threshold of the proposed GLRT $\widehat{\delta}_2(\mathbf{Z})$ is given by:

$$\widehat{\tau}_2 = \Phi^{-1}(1 - \alpha_0), \quad (43)$$

Proposition 4: On the assumption that the pixels are modeled by the proposed enhanced Poissonian-Gaussian model (6), when the camera parameters $(a_{k,j}, b_{k,j})$ are known and the pixels' expectations $\widehat{\mu}_k$ are estimated as in (27), for any decision threshold $\widehat{\tau}_2$, the power function associated with test $\widehat{\delta}_2$ (38) is given by

$$\beta_{\widehat{\delta}_2} = 1 - \Phi\left(\frac{\sigma'_0}{\sigma'_1} \cdot \widehat{\tau}_2 + \frac{m'_0 - m'_1}{\sigma'_1}\right). \quad (44)$$

Again, the main advantages of the proposed GLRT $\widehat{\delta}_2(\mathbf{Z})$ are that 1) one can analytically establish its statistical performance and hence easily calculate the decision threshold with guaranteeing a prescribed false alarm probability, and ensuing the power function; 2) due to the normalization, the calculated decision threshold can only depend on the prescribed false alarm probability α_0 .

C. DISCUSSION OF THIS GLRT

In some operational cases, the camera parameter $(a_{k,j}, b_{k,j})$ might not be available during the forensic investigation. In such a case, it is proposed to replace the camera parameter $(a_{k,j}, b_{k,j})$ by their estimates denoted $(\widehat{a}_{k,j}, \widehat{b}_{k,j})$, as given in Equations (32) and (33). Since the limitation of binary classification, it also should be noted that relying on the proposed GLRT, the inspected image \mathbf{Z} is either captured with device \mathcal{S}_0 or with device \mathcal{S}_1 . In other words, the proposed test cannot be directly applied for images acquired with another different instance. To overcome that limitation, in the following section, let us design a more practical multi-classifier to deal with the problem of identifying multiple camera devices.

V. DESIGN OF MULTI-CLASSIFIER

Although the GLRT is successfully capable of identifying between individual device \mathcal{S}_0 and \mathcal{S}_1 , it hardly holds true that the signal detector can deal with the problem of multi-classification, which to some extent limits the application of our proposed algorithm. Therefore, in this section, let us extend the binary classifier, namely signal GLRT, to a more practical multi-classifier for identifying multiple devices.

To solve the problem of multi-classification, one has to assign each of the observations, referring to as an inquiry image \mathbf{Z} , into one of Y classes (individual cameras). Let us define a set $\mathcal{S} = \{\mathcal{S}_y\}$ where $y \in \{1, \dots, Y\}$. In addition, it is proposed to consider two practical scenarios: in the first scenario, all the classes are known, where the designed multi-classifier can only identify the inquiry images from the known camera devices, and meanwhile fails to detect images acquired by an unknown camera; in the second scenario, the multi-classifier cannot only identify images captured by known camera devices, but also unknown devices.

A common way to establish our practical multi-classifier is by combining multiple binary/sub classifiers with the voting strategy. In this context, we select each normalized

GLRT $\widehat{\delta}_2^{(n_{\text{sub}})}(\mathbf{Z})$ (38) as a sub classifier, which is re-defined as:

$$\widehat{\delta}_2^{(n_{\text{sub}})}(\mathbf{Z}) = \begin{cases} \mathcal{H}_0 & \text{if } \widehat{\Lambda}_2^{(n_{\text{sub}})}(\mathbf{Z}) < \widehat{\tau}_2, \\ \mathcal{H}_1 & \text{if } \widehat{\Lambda}_2^{(n_{\text{sub}})}(\mathbf{Z}) \geq \widehat{\tau}_2. \end{cases} \quad (45)$$

where one can assume \mathbf{Z} is acquired by \mathcal{S}_y under hypothesis \mathcal{H}_0 while $\mathcal{S}_{y'}$ under hypothesis \mathcal{H}_1 , or \mathcal{S}_y under hypothesis \mathcal{H}_1 while $\mathcal{S}_{y'}$ under hypothesis \mathcal{H}_0 . It should be noted that $y' \in \{1, \dots, Y\}$ is different from y . Then, the sub classifier index is defined as $n_{\text{sub}} \in \{1, \dots, N_{\text{sub}}\}$, where N_{sub} can be formulated by:

$$N_{\text{sub}} = Y \times (Y - 1) \quad (46)$$

denoting the total number of the sub classifiers, where $Y \geq 3$ denotes the whole number of all the individual devices in the known close set \mathcal{S} . Thus, the number of sub classifiers is even, and meanwhile our designed multi-classifier contains $\frac{N_{\text{sub}}}{2}$ pairwise symmetric $\widehat{\delta}_2^{(n_{\text{sub}})}$. It should be noted that due to the normalization of the GLRT, the threshold $\widehat{\tau}_2$ remains the same for each sub classifier, regardless of \mathcal{S}_y .

In fact, if \mathbf{Z} is captured by an element of \mathcal{S} , which is a close set, our proposed multi-classifier is required to deal with the first identification scenario; if some inquiry images are not from any element of \mathcal{S} , it belongs to an open set containing \mathcal{S} , leading to the second scenario of source camera identification (see [47], [48] for details). Regardless of close or open set, our established multi-classifier consists of the same sub classifiers with the same number. By modifying the voting strategy, we can smoothly switch our multi-classifier to deal with two practical scenarios.

In the close set, for simplicity, we adopt the strategy of plurality voting, which is described as:

$$\begin{cases} v_{\mathcal{S}_y} = v_{\mathcal{S}_y} + 1 & \text{if } \mathbf{Z} \text{ is identified from } \mathcal{S}_y \text{ by } \widehat{\delta}_2^{(n_{\text{sub}})} \\ v_{\mathcal{S}_{y'}} = v_{\mathcal{S}_{y'}} + 1 & \text{else} \end{cases}$$

where the voting vector $\mathbf{v} = \{v_{\mathcal{S}_1}, \dots, v_{\mathcal{S}_Y}\}$ is used for counting the number of each identification. For each sub classifier, one is required to update the value of both $v_{\mathcal{S}_y}$ and $v_{\mathcal{S}_{y'}}$ with their initial value equal to zero. Then let us calculate the index value:

$$Ind = \text{Max}(\mathbf{v}) \quad (47)$$

to obtain the final identification \mathcal{S}_{Ind} , where the function $\text{Max}(\cdot)$ calculates the index value of the maximum of \mathbf{v} .

In the open set, \mathbf{Z} is possibly captured by an unknown device. In our multi-classifier, each sub classifier is prone to classify it into the class under hypothesis \mathcal{H}_0 . Therefore, before calculating the index value Ind , let us give the prerequisite: if \mathbf{Z} is identified from \mathcal{S} under hypothesis \mathcal{H}_0 by all sub classifiers, our multi-classifier directly identifies \mathbf{Z} acquired by an unknown camera device. Relying on each reliable sub classifier with an equal weight, our proposed multi-classifier cannot only deal with the problem of source camera identification in the close set, but also in the open set. Meanwhile, the detection power is empirically validated in the following extensive experiments.

VI. NUMERICAL EXPERIMENTS

A. RESULTS ON SIMULATED IMAGES FOR RAW FORMAT

To verify the sharpness of the theoretically established results, let us adopt a Monte Carlo simulation on a 8-bit synthetic image of size 512×512 (see Fig. 4) with 3000 repetitions. Note that it is proposed to normalize the synthetic image into the interval $[0, 1]$. In our simulated experiments, we simulate 256 level sets. Thus, device \mathcal{S}_0 and \mathcal{S}_1 can be respectively characterized by using 256 pairs of camera parameters of $(a_{k,0}, b_{k,0})$ and $(a_{k,1}, b_{k,1})$, $k \in \{1, \dots, 256\}$. As Fig. 5 illustrates, we use a Receiver Operating Character (ROC) to demonstrate the detection power $\beta_{\bar{\delta}^{lr}}$ as a function of the false alarm probability α_0 , where $I = \{40, 60, 80, 100\}$ denotes the number of pixels used in our proposed test $\bar{\delta}^{lr}$ (18). By using our proposed algorithms (see details in Section IV), the camera parameters and the pixels' expectations are successfully predicted prior to the testing. By observation, with increasing the number of pixels, our proposed test performs better and better. Furthermore, due to the utilization of the more accurate model for establishing the LRT, our designed LRT remarkably outperforms the LRT of [34].

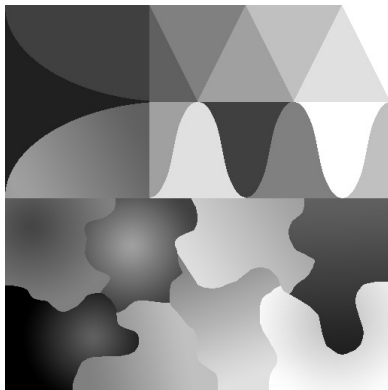


FIGURE 4. Illustration of a synthetic image of size 512×512 .

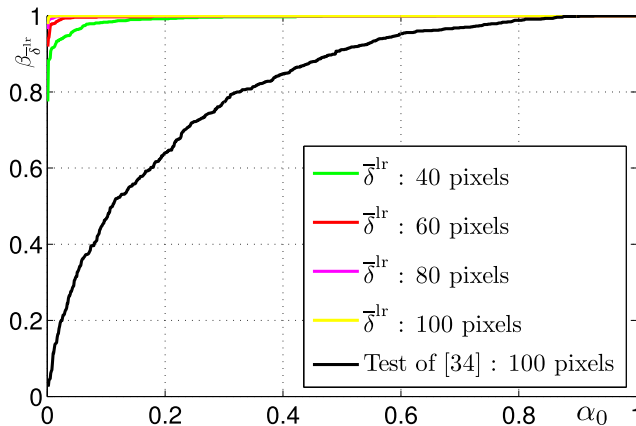
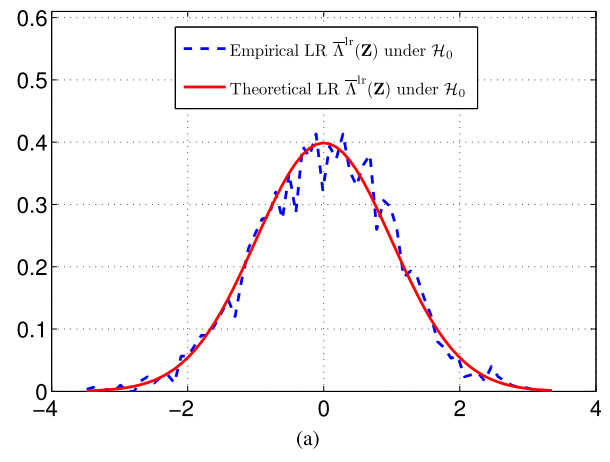


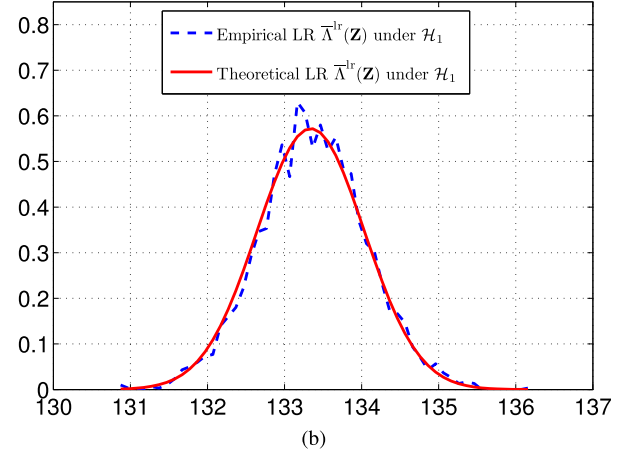
FIGURE 5. Detection performance of the test $\bar{\delta}^{lr}$ and its counterpart of [34] with assuming the known camera and image parameters on simulated images.

To verify the effectiveness of the established LRT $\bar{\delta}^{lr}$, again, it is proposed to adopt a Monte-Carlo simulation by repeating 3000 times using all the pixels for each synthetic

image. Fig 6a demonstrates the distribution of the empirical $\bar{\Lambda}^{lr}(\mathbf{Z})$ under hypothesis \mathcal{H}_0 . Meanwhile, let us plot the theoretical pdf of $\bar{\Lambda}^{lr}(\mathbf{Z})$ following the standard Gaussian distribution with zero mean and unit variance. Similarly, under hypothesis \mathcal{H}_1 , empirical and theoretical distribution of $\bar{\Lambda}^{lr}(\mathbf{Z})$ are demonstrated in Fig 6b. Note that the theoretical pdf of $\bar{\Lambda}^{lr}(\mathbf{Z})$ follows the Gaussian distribution with the mean $\frac{m_1 - m_0}{\sigma_0}$ and the variance $\frac{\sigma_1^2}{\sigma_0^2}$. The results of Fig. 6 directly verify the accuracy of the theoretically established distribution of the proposed LR, and the statistical remarkable performance of the LRT (18).



(a)



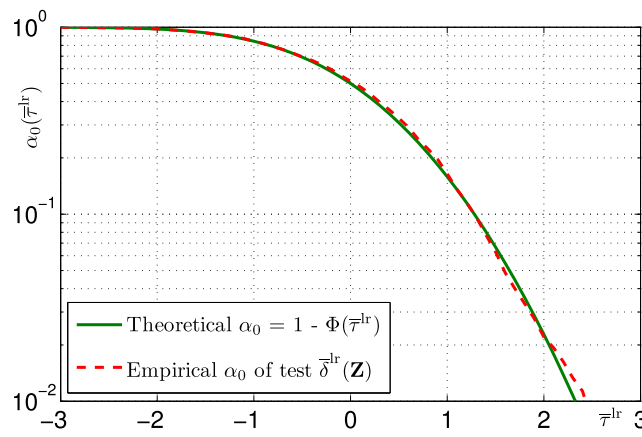
(b)

FIGURE 6. Comparison between empirical and theoretical distribution of $\bar{\Lambda}^{lr}(\mathbf{Z})$ under hypothesis \mathcal{H}_0 and hypothesis \mathcal{H}_1 . (a) Under \mathcal{H}_0 . (b) Under \mathcal{H}_1 .

This paper aims to establish a statistical test with warranting a prescribed false alarm probability. Therefore, we compare the empirical false alarm probability with the theoretically established one for the test (18) as a function of the threshold $\bar{\tau}^{lr}$ (see Fig. 7). Fig. 7 reports that the empirical result perfectly matches the theoretical false alarm probability, which confirms the ability of the proposed LRT to guarantee a prescribed false alarm probability in practice. In some cases ($\bar{\tau}^{lr} \geq 2$), the inaccuracy of the CLT for modeling tails might lead to the slight differences of two curves.

TABLE 1. Image dataset statistic in RAW format.

Database Type	Camera Model/Device	Alias	Sensor size	Native resolution	Bit depth	ISO sensitivity	No. images
Dresden [39]	Nikon D70 # 0	N_D70_0	23.7 × 15.6 mm CCD	2014 × 3039	12	200	180
	Nikon D70 # 1	N_D70_1	23.7 × 15.6 mm CCD	2014 × 3039	12	200	189
	Nikon D70s # 0	N_D70s_0	23.7 × 15.6 mm CCD	2014 × 3039	12	200	178
	Nikon D70s # 1	N_D70s_1	23.7 × 15.6 mm CCD	2014 × 3039	12	200	189
	Nikon D200 # 0	N_D200_0	23.6 × 15.8 mm CCD	2616 × 3900	12	200	372
	Nikon D200 # 1	N_D200_1	23.6 × 15.8 mm CCD	2616 × 3900	12	200	380
Our own data	Canon 100D # 0	C_100D_0	22.3 × 14.9 mm CMOS	3528 × 5280	14	100-200-400	200-317-220
	Canon 100D # 1	C_100D_1	22.3 × 14.9 mm CMOS	3528 × 5280	14	100-200-400	200-389-220
	Pentax K-50 # 0	P_K50_0	23.7 × 15.7 mm CMOS	3272 × 4936	12	100-200-400	300-269-220
	Pentax K-50 # 1	P_K50_1	23.7 × 15.7 mm CMOS	3272 × 4936	12	100-200-400	300-211-220
	Nikon D5200 # 0	N_D5200_0	23.5 × 15.6 mm CMOS	4020 × 6036	14	100-200-400	300-300-250
	Nikon D5200 # 1	N_D5200_1	23.5 × 15.6 mm CMOS	4020 × 6036	14	100-200-400	300-755-250
$\sum 2$		12	12	5	5	2	3
							6709

**FIGURE 7.** Comparison between the theoretical false alarm probability α_0 and its empirical values, plotted as a function of the threshold τ^{lr} .

B. RESULTS ON REAL IMAGES FOR RAW FORMAT

Finally, it is necessary that we have to test the effectiveness of our proposed algorithm over the real data. The experimental dataset consists of the benchmark Dresden image database [39] and our own database. In Dresden database, we select all full-resolution images from the three following camera models *Nikon D70*, *Nikon D70s* and *Nikon D200*, where for each camera model the Dresden database provides images captured by two different devices. To enrich camera models of the experimental dataset, it is proposed to add our own three camera models: *Canon 100D*, *Pentax K-50* and *Nikon D5200*. Table 1 reports the specific parameter settings of the each camera in the experimental dataset. By using the software *Ddraw* (with parameters -D -4 -j -v -r 1 1 1 1, one can obtain a full-resolution image on 12 or 14 bits, depending on the camera model, without any processing.), one can convert each RAW format image into an uncompressed one, and decompress it into 4 sub-images, where only the red color channel⁵ is used. Additionally, note that our model is sensitive to the ISO which is presented as the same value (100/200/400 in our experiments) before capturing an image (see details in Section II).

⁵The red color channel is selected arbitrarily; the blue or green color channel can obtain similar results.

First, let us divide each set of images from each device into two subsets: “*Learning Subset*” and “*Testing Subset*”. Images of “*Learning Subset*” are used to extract camera fingerprints from each device; images of “*Testing Subset*” are used to identify the origin of an image under investigation. Note that “*Learning Subset*” and “*Testing Subset*” are disjoint, that is none of images are used for estimating camera device parameters and meanwhile for testing. The number of “*Learning Subset*” is set as 50, which is a good compromise between computation efficiency and estimation accuracy. In our experiments for evaluating the performance of the GLRT, each model has two devices: \mathcal{S}_0 and \mathcal{S}_1 which respectively represents the hypotheses \mathcal{H}_0 and \mathcal{H}_1 .

To our knowledge, few camera identification methods work on images in RAW format. Based on the Poissonian-Gaussian noise model (3), the test of [35] opens the way of studying the problem of identifying source camera model, relying on RAW data. Thus, let us compare our test with the detector of [35]. In addition, to verify that the proposed detector designed using the model (6) outperforms our prior detector of [34], we also compare the results from those two detectors. Fig. 8 reports that our proposed detector performs very well with the considerable ability of identifying source camera device. By contrast, the ROC curves of the detector [35] perform, roughly speaking, a “random guess”, since the power function approximatively equals the false alarm probability. Therefore, it is incapable of identifying the individual camera device. On the assumption that parameter b_k remains slightly varied for each level set, instead of the constant b from the model proposed in [34], we use more accurate algorithm for estimating parameter (a_k, b_k) (see Equations (32) and (33) for details). Thus, our proposed novel estimation algorithm and model parameters, different from those of [34], directly result into the remarkably improved accuracy of classifying the individual camera device, especially in the case of prescribing the small α_0 .

Furthermore, by using images acquired by all camera devices in the dataset, let us present the detection performance. The results are illustrated in Fig. 9. Depending on the enhanced Poissonian-Gaussian noise model (6),

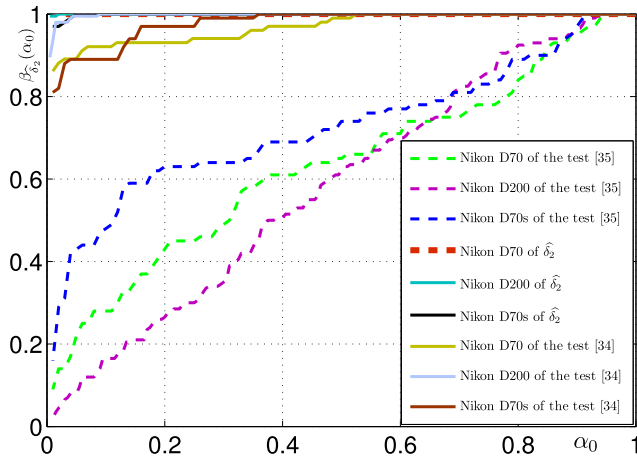


FIGURE 8. Detection performance of the test $\hat{\delta}_2$: parameters $(a_{k,0}, b_{k,0})$ of S_0 and $(a_{k,1}, b_{k,1})$ of S_1 are known, μ_k are unknown on real images. Note that for each camera model, the test $\hat{\delta}_2$ is designed for identifying the inspected image Z acquired by S_0 or S_1 , which both belongs to the same model.

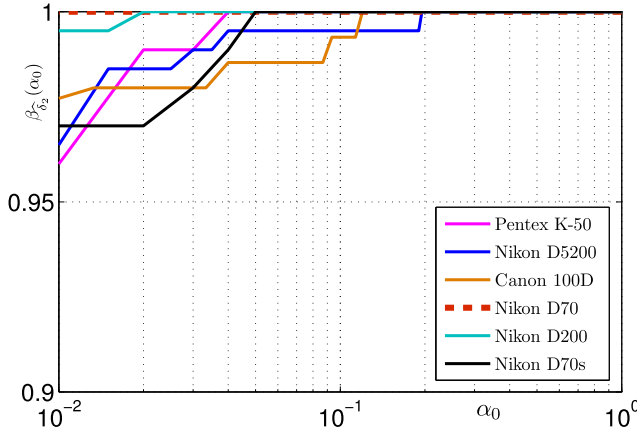


FIGURE 9. Comparison of detection performance on a large scale database (logarithmic scale).

ROC curves demonstrate the relevance of our designed detector.

Besides, let us compare the proposed test with the prior-art detector of [27]. For fair comparison, still, we propose to use 50 images from “*Learning Subset*”, and calculate a reference PRNU as the fingerprint of the camera device S_0 . Then the Peak to Correlation Energy (PCE), used for “*Testing Subset*”, is computed to detect if the inspected image is acquired with the device S_0 . Besides, it is proposed to use the usual criteria of minimal Probability of Error (or P_E for short). This performance criterion denotes the minimal value of false alarm and missed detection probability, which is formulated by:

$$P_E = \min_{\alpha_0 \in (0,1)} \frac{\alpha_0 + (1 - \beta_{\hat{\delta}_2})}{2}. \quad (48)$$

Table 2 compares the empirical performance, via P_E criterion, of our proposed test, the test proposed in [35] and

TABLE 2. Minimal P_E comparison, assuming that two devices S_0 and S_1 from the same camera model.

Camera Model	Proposed Test $\hat{\delta}_2$	Test [35]	Test [27]
Nikon D70	0.005	0.380	0.015
Nikon D70s	0.020	0.325	0.005
Nikon D200	0.005	0.417	0.002
Canon 100D	0.016	0.347	0.020
Pentax K-50	0.015	0.355	0.020
Nikon D5200	0.015	0.560	0.005
Average	0.012	0.397	0.011

the prior-art test of [27]. Note that the results illustrated in Table 2 are for identifying two different devices of each tested model. Obviously, this table demonstrates that the test proposed in [35], relying on the Poissonian-Gaussian noise model, is incapable of identifying each instance, while our proposed test based on the enhanced Poissonian-Gaussian noise performs comparably to the test of [27]. For instance, to identify the camera device *Nikon D70*, *Canon 100D*, and *Pentax K-50*, our proposed detector outperforms the one proposed in [27].

In virtue of the same experimental dataset and the same tests, the results of Table 3 compares the empirical power for a fixed false alarm probability of α_0 . By observation, this table also shows that our proposed methodology and the state-of-the-art detector of [27] exhibit roughly the same performance. Moreover, to verify the effectiveness of our proposed test in the case of different ISO values, Table 4 illustrates that our proposed detector performs very well with different ISO settings.

TABLE 3. Detection power (true positive rate) comparison at the given false alarm probability α_0 , assuming that two devices S_0 and S_1 from the same camera model. (a) $\alpha_0 = 0.05$. (b) $\alpha_0 = 0.01$.

(a)			
Camera Model	Proposed Test $\hat{\delta}_2$	Test [35]	Test [27]
Nikon D70	1.00	0.25	1.00
Nikon D70s	1.00	0.34	1.00
Nikon D200	1.00	0.11	1.00
Canon 100D	0.98	0.22	0.96
Pentax K-50	1.00	0.19	0.97
Nikon D5200	0.99	0.28	0.99
Average	0.99	0.23	0.98

(b)			
Camera Model	Proposed Test $\hat{\delta}_2$	Test [35]	Test [27]
Nikon D70	1.00	0.09	0.96
Nikon D70s	0.97	0.15	1.00
Nikon D200	1.00	0.01	1.00
Canon 100D	0.97	0.12	0.96
Pentax K-50	0.96	0.11	0.97
Nikon D5200	0.97	0.01	0.99
Average	0.98	0.08	0.98

In the practical identification, our detector is not only capable of identifying the source camera device from the same model, but also from different camera models.

TABLE 4. Detection power comparison at the given false alarm probability α_0 , assuming that two devices S_0 and S_1 from the same camera model with different ISO settings. (a) $\alpha_0 = 0.05$. (b) $\alpha_0 = 0.01$.

(a)

Camera Model	ISO = 100	ISO = 200	ISO = 400
Canon 100D	0.96	0.98	1.00
Pentax K-50	0.99	1.00	0.99
Nikon D5200	0.96	0.99	1.00
Average	0.97	0.99	1.00

(b)

Camera Model	ISO = 100	ISO = 200	ISO = 400
Canon 100D	0.96	0.98	1.00
Pentax K-50	0.99	0.99	0.99
Nikon D5200	0.94	0.99	1.00
Average	0.96	0.99	1.00

TABLE 5. Detection power comparison between N_D70_0 under hypothesis \mathcal{H}_0 and the selected devices from different models of the same camera brand under hypothesis \mathcal{H}_1 at the given false alarm probability α_0 . (a) $\alpha_0 = 0.05$. (b) $\alpha_0 = 0.01$.

(a)

Camera Model	Proposed Test $\hat{\delta}_2$	Test [35]	Test [27]
N_D70s_0	1.00	0.11	0.99
N_D70s_1	0.97	0.25	1.00
N_D200s_0	1.00	0.66	1.00
N_D200s_1	0.99	0.57	1.00
Average	0.99	0.39	1.00

(b)

Camera Model	Proposed Test $\hat{\delta}_2$	Test [35]	Test [27]
N_D70s_0	0.99	0.11	0.97
N_D70s_1	0.90	0.25	0.99
N_D200s_0	0.98	0.66	0.99
N_D200s_1	0.99	0.57	0.99
Average	0.97	0.24	0.99

Then, Table 5 and 6 respectively report the comparison results, which empirically verify that our proposed test obviously outperforms the detector of [35], and very comparable to the prior-art detector of [27].

Next, it is proposed to verify the effectiveness of our multi-classifier. We randomly select 100 images from each individual device, constituting the “Learning Subset” for evaluating the performance of our proposed multi-classifier. Table 7 illustrates the confusion matrix (consisting of probabilities) of detection performance using our proposed multi-classifier. In a confusion matrix, each column of the matrix represents the individual camera device in a close set \mathcal{S} while each row (the identification result) represents the one in the predicted class. Note that the correct rate (referring to as the probabilities along the main diagonal) is defined as the correctly predicted result. As Table 7 reports, in the close set including three individual devices (two different models), our proposed multi-classifier can perfectly identify N_D70_0, and N_D200_0 with tiny error. However, the detection performance for N_D70_1 with 83% correct rate is not as well as the others.

TABLE 6. Detection power comparison between N_D70_1 under hypothesis \mathcal{H}_0 and the selected devices from different camera brands under hypothesis \mathcal{H}_1 at the given false alarm probability α_0 . (a) $\alpha_0 = 0.05$. (b) $\alpha_0 = 0.01$.

(a)

Camera Model	Proposed Test $\hat{\delta}_2$	Test [35]	Test [27]
P_K50_0	1.00	0.56	0.99
P_K50_1	1.00	0.59	1.00
C_100D_0	1.00	0.93	1.00
C_100D_1	1.00	0.91	1.00
Average	1.00	0.75	0.99

(b)

Camera Model	Proposed Test $\hat{\delta}_2$	Test [35]	Test [27]
P_K50_0	1.00	0.44	0.96
P_K50_1	1.00	0.47	0.97
C_100D_0	1.00	0.63	1.00
C_100D_1	1.00	0.25	1.00
Average	1.00	0.45	0.98

TABLE 7. Confusion matrix of our proposed multi-classifier in the close set.

	N_D70_0	N_D70_1	N_D200_0
N_D70_0	1.00	0.00	0.00
N_D70_1	0.16	0.83	0.01
N_D200_0	0.01	0.00	0.99

Additionally, we propose to verify the effectiveness of our multi-classifier in an open set. Three individual devices are known (N_D70_0, N_D70_1, and N_D200_0) while one device (N_D200_1) unknown. Note that when identifying an unknown device, our multi-classifier cannot acquire any camera fingerprint of it. As Table 8 illustrates, our multi-classifier remains its performance with high correct rate for dealing with known candidate devices in the set \mathcal{S} , and meanwhile is capable of identifying un unknown device not from \mathcal{S} , where the correct rate arrives at 84%. Furthermore, when mixed (more than one) unknown devices are required to be identified, for instance N_D200_1 plus P_K50_0, our multi-classifier can still classify images captured by unknown cameras with its correct rate 86%. Since each sub classifier cannot acquire any fingerprint from unknown samples, the identification result of it is prone to the class under hypothesis \mathcal{H}_0 . The empirical results straightforward verify that relying on our designed voting strategy (see Sec. V), the multi-classifier can identify images acquired by unknown devices with acceptable prediction error.

TABLE 8. Confusion matrix of our proposed multi-classifier in the open set.

	N_D70_0	N_D70_1	N_D200_0	Unknown device
N_D70_0	1.00	0.00	0.00	0.00
N_D70_1	0.07	0.83	0.01	0.09
N_D200_0	0.01	0.00	0.99	0.00
Unknown device	0.05	0.01	0.10	0.84

TABLE 9. Comparison results from two confusion matrices in the close set.

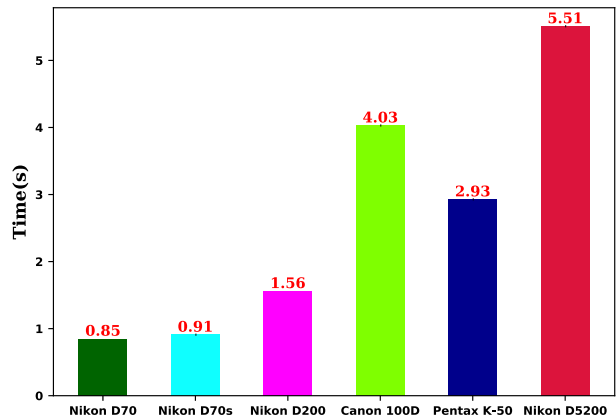
	N_D70_0	N_D70_1	N_D70s_0	N_D70s_1
N_D70_0	0.98, 0.28	0.00, 0.24	0.00, 0.39	0.02, 0.09
N_D70_1	0.10, 0.28	0.79, 0.30	0.00, 0.36	0.11, 0.06
N_D70s_0	0.03, 0.31	0.00, 0.25	0.95, 0.35	0.02, 0.09
N_D70s_1	0.02, 0.31	0.00, 0.25	0.03, 0.36	0.95, 0.08

To furthermore validate our proposed algorithm, let us compare the multi-classifier with a Convolutional Neural Network (CNN) based classifier proposed in [49]. Next, it is proposed to establish the testing set including two models with four individual devices. Then two confusion matrices are illustrated in Table 9. Along the main diagonal, the correct rates acquired by two detectors are demonstrated, where for each device the results of the first column are obtained from our multi-classifier while the second column is acquired from that of [49]. It can be observed that our detector remarkably outperforms the prior art. Because the detector of [49] can only identify camera models, not individual devices. Besides, the sensor equipped by Nikon D70 is identical to that of Nikon D70s (see [39]), leading to that two camera models are hardly discriminated by using a camera model detector. By contrast, our proposed multi-classifier with the ability of identifying individual camera device can effectively classify those devices.

VII. CONCLUSION AND LIMITATION

In this context, we mainly investigate the problem of identifying the source camera device. In current literature, the detectors relying on the PRNU features nearly dominate the research of source camera identification. However, in this paper, we novelly use an enhanced Poissonian-Gaussian noise model to design the test. Depending on this new model, the problem of identification can be cast in the framework of the hypothesis testing theory. The main contribution of this paper is the designing of the optimal LRT, the practical GLRT, and the multi-classifier. First, on the assumption that the camera fingerprints and image parameters are perfectly known, we propose to design the LRT, and meanwhile analytically establish its statistical performance. Second, in the practical scenario, based on the estimated image parameters, we establish the practical GLRT with remarkable performance. Third, by combining GLRTs with the voting strategy, the multi-classifier performs effectively. To our knowledge, the proposed test in this paper is the only statistical detector of identifying individual camera device based on RAW images. Thus, this paper enriches the forensic research in this field.

The main limitation of the proposed algorithm is that camera fingerprints from RAW format require the ISO value. In addition, if the number of individual camera for identification is increased, it is required to enlarge Y (the amount of sub classifier), leading to reduction of detection efficiency and increment of overall computation time. Fig. 10 reports

**FIGURE 10.** Illustration of computation time for each image from different camera models.

the detailed computation time for an image from different models. Due to the same size of an image acquired by Nikon D70 or D70s, the average time cost basically remains the same. With increasing the size of an inspected image preset by a given camera, the computation time is enhanced. Thus, regardless of camera models, the deterministic parameter of the computation time is image size. Nevertheless, to deal with an inquiry image by each sub classifier, the computation time is acceptable. By using MATLAB R2015B, all our experiments are implemented on a PC with 32 CPUs of Intel Xeon E7-4820 2.00GHz.

Considering the post-processing such as demosaicing, white balancing, and gamma correction (see Fig. 1), we are capable of extending our proposed model from RAW to JPEG images. In fact, the linear transform including demosaicing and white balancing nearly cannot interfere the extracted noise while the non-linear gamma correction to some extent impacts our proposed noise model in this context. Thus, the statistical noise model has to be re-established while the relationship between model parameters is re-assumed. Besides, model parameters of the JPEG image are estimated based on the 8×8 image blocks, instead of the level sets of this context. Thus, the new LRT and GLRT are both designed. A specific method for JPEG images has been proposed in [50] and [51].

REFERENCES

- [1] H. T. Sencar and N. Memon, *Digital Image Forensics: There is More to a Picture than Meets the Eye*. New York, NY, USA: Springer, 2012.
- [2] M. C. Stamm, M. Wu, and K. J. R. Liu, “Information forensics: An overview of the first decade,” *IEEE Access*, vol. 1, pp. 167–200, 2013.
- [3] V. Christlein, C. Riess, J. Jordan, C. Riess, and E. Angelopoulou, “An evaluation of popular copy-move forgery detection approaches,” *IEEE Trans. Inf. Forensics Security*, vol. 7, no. 6, pp. 1841–1854, Dec. 2012.
- [4] Y.-F. Hsu and S.-F. Chang, “Camera response functions for image forensics: An automatic algorithm for splicing detection,” *IEEE Trans. Inf. Forensics Security*, vol. 5, no. 4, pp. 816–825, Dec. 2010.
- [5] T. Qiao, A. Zhu, and F. Retraint, “Exposing image resampling forgery by using linear parametric model,” *Multimedia Tools Appl.*, vol. 77, no. 2, pp. 1501–1523, 2017.

- [6] T. Qiao, R. Shi, X. Luo, M. Xu, N. Zheng, and Y. Wu, "Statistical model-based detector via texture weight map: Application in re-sampling authentication," *IEEE Trans. Multimedia*, Oct. 2018, doi: [10.1109/TMM.2018.2872863](https://doi.org/10.1109/TMM.2018.2872863).
- [7] M. C. Stamm and K. J. R. Liu, "Forensic detection of image manipulation using statistical intrinsic fingerprints," *IEEE Trans. Inf. Forensics Security*, vol. 5, no. 3, pp. 492–506, Sep. 2010.
- [8] Z. Fan and R. L. de Queiroz, "Identification of bitmap compression history: JPEG detection and quantizer estimation," *IEEE Trans. Image Process.*, vol. 12, no. 2, pp. 230–235, Feb. 2003.
- [9] X. Kang, M. C. Stamm, A. Peng, and K. J. R. Liu, "Robust median filtering forensics using an autoregressive model," *IEEE Trans. Inf. Forensics Security*, vol. 8, no. 9, pp. 1456–1468, Sep. 2013.
- [10] X. Jiang, S. Wei, R. Zhao, Y. Zhao, and X. Wu. (Oct. 2016). "Camera fingerprint: A new perspective for identifying user's identity." [Online]. Available: <https://arxiv.org/abs/1610.07728>
- [11] D. Valsesia, G. Coluccia, T. Bianchi, and E. Magli, "Large-scale image retrieval based on compressed camera identification," *IEEE Trans. Multimedia*, vol. 17, no. 9, pp. 1439–1449, Sep. 2015.
- [12] X. Lin and C.-T. Li, "Large-scale image clustering based on camera fingerprints," *IEEE Trans. Inf. Forensics Security*, vol. 12, no. 4, pp. 793–808, Apr. 2017.
- [13] I. Amerini, R. Caldelli, P. Crescenzi, A. D. Mastio, and A. Marino, "Blind image clustering based on the Normalized Cuts criterion for camera identification," *Signal Process. Image Commun.*, vol. 29, no. 8, pp. 831–843, 2014.
- [14] J. Nakamura, *Image Sensors and Signal Processing for Digital Still Cameras*. Boca Raton, FL, USA: CRC Press, 2005.
- [15] R. Ramanath, W. E. Snyder, Y. Yoo, and M. S. Drew, "Color image processing pipeline," *IEEE Signal Process. Mag.*, vol. 22, no. 1, pp. 34–43, Jan. 2005.
- [16] Z. Deng, A. Gijsenij, and J. Zhang, "Source camera identification using auto-white balance approximation," in *Proc. IEEE Int. Conf. Comput. Vis. (ICCV)*, Nov. 2011, pp. 57–64.
- [17] K. S. Choi, E. Y. Lam, and K. K. Y. Wong, "Source camera identification using footprints from lens aberration," *Proc. SPIE*, vol. 6069, p. 60690J, Feb. 2006.
- [18] S. Bayram, H. Sencar, N. Memon, and I. Avcibas, "Source camera identification based on CFA interpolation," in *Proc. IEEE Int. Conf. Image Process. (ICIP)*, vol. 3, Sep. 2005, p. III-69.
- [19] H. Cao and A. C. Kot, "Accurate detection of demosaicing regularity for digital image forensics," *IEEE Trans. Inf. Forensics Security*, vol. 4, no. 4, pp. 899–910, Dec. 2009.
- [20] M. Kharrazi, H. T. Sencar, and N. Memon, "Blind source camera identification," in *Proc. Int. Conf. Image Process. (ICIP)*, vol. 1, Oct. 2004, pp. 709–712.
- [21] A. Swaminathan, M. Wu, and K. J. R. Liu, "Nonintrusive component forensics of visual sensors using output images," *IEEE Trans. Inf. Forensics Security*, vol. 2, no. 1, pp. 91–106, Mar. 2007.
- [22] K. S. Choi, E. Y. Lam, and K. K. Y. Wong, "Source camera identification by JPEG compression statistics for image forensics," in *Proc. IEEE Region 10 Conf. TENCON*, Nov. 2006, pp. 1–4.
- [23] C. Scott, "Performance measures for Neyman–Pearson classification," *IEEE Trans. Inf. Theor.*, vol. 53, no. 8, pp. 2852–2863, Aug. 2007.
- [24] J. R. Janesick, *Scientific Charge-Coupled Devices*, vol. 117. Bellingham, WA, USA: SPIE, 2001.
- [25] J. Lukáš, J. Fridrich, and M. Goljan, "Digital camera identification from sensor pattern noise," *IEEE Trans. Inf. Forensics Security*, vol. 1, no. 2, pp. 205–214, Jun. 2006.
- [26] M. Chen, J. Fridrich, M. Goljan, and J. Lukás, "Determining image origin and integrity using sensor noise," *IEEE Trans. Inf. Forensics Security*, vol. 3, no. 1, pp. 74–90, Mar. 2008.
- [27] M. Goljan, J. Fridrich, and T. Filler, "Large scale test of sensor fingerprint camera identification," *Proc. SPIE*, vol. 7254, p. 72540I, Feb. 2009.
- [28] C.-T. Li and Y. Li, "Color-decoupled photo response non-uniformity for digital image forensics," *IEEE Trans. Circuits Syst. Video Technol.*, vol. 22, no. 2, pp. 260–271, Feb. 2012.
- [29] X. Kang, Y. Li, Z. Qu, and J. Huang, "Enhancing source camera identification performance with a camera reference phase sensor pattern noise," *IEEE Trans. Inf. Forensics Security*, vol. 7, no. 2, pp. 393–402, Apr. 2012.
- [30] K. Kurosawa, K. Kuroki, and N. Saitoh, "CCD fingerprint method-identification of a video camera from videotaped images," in *Proc. Int. Conf. Image Process. (ICIP)*, vol. 3, Oct. 1999, pp. 537–540.
- [31] T. Filler, J. Fridrich, and M. Goljan, "Using sensor pattern noise for camera model identification," in *Proc. 15th IEEE Int. Conf. Image Process. (ICIP)*, Oct. 2008, pp. 1296–1299.
- [32] T. Gloe, M. Kirchner, A. Winkler, and R. Böhme, "Can we trust digital image forensics?" in *Proc. ACM 15th Int. Conf. Multimedia*, 2007, pp. 78–86.
- [33] R. Li, C.-T. Li, and Y. Guan, "Inference of a compact representation of sensor fingerprint for source camera identification," *Pattern Recognit.*, vol. 74, pp. 556–567, Feb. 2018.
- [34] T. Qiao, F. Retraint, R. Cogranne, and T. H. Thai, "Source camera device identification based on raw images," in *Proc. IEEE Int. Conf. Image Process. (ICIP)*, Sep. 2015, pp. 3812–3816.
- [35] T. H. Thai, R. Cogranne, and F. Retraint, "Camera model identification based on the heteroscedastic noise model," *IEEE Trans. Image Process.*, vol. 23, no. 1, pp. 250–263, Jan. 2014.
- [36] A. Foi, M. Trimeche, V. Katkovnik, and K. Egiazarian, "Practical Poissonian–Gaussian noise modeling and fitting for single-image raw-data," *IEEE Trans. Image Process.*, vol. 17, no. 10, pp. 1737–1754, Oct. 2008.
- [37] A. Foi, "Clipped noisy images: Heteroskedastic modeling and practical denoising," *Signal Process.*, vol. 89, no. 12, pp. 2609–2629, 2009.
- [38] G. E. Healey and R. Kondepudy, "Radiometric CCD camera calibration and noise estimation," *IEEE Trans. Pattern Anal. Mach. Intell.*, vol. 16, no. 3, pp. 267–276, Mar. 1994.
- [39] T. Gloe and R. Böhme, "The dresden image database for benchmarking digital image forensics," *J. Digit. Forensic Pract.*, vol. 3, nos. 2–4, pp. 150–159, 2010.
- [40] E. L. Lehmann and J. P. Romano, *Testing Statistical Hypotheses*. Berlin, Germany: Springer, 2006.
- [41] R. Cogranne and F. Retraint, "An asymptotically uniformly most powerful test for LSB matching detection," *IEEE Trans. Inf. Forensics Security*, vol. 8, no. 3, pp. 464–476, Mar. 2013.
- [42] R. Cogranne, C. Zitzmann, F. Retraint, I. V. Nikiforov, P. Cornu, and L. Fillatre, "A local adaptive model of natural images for almost optimal detection of hidden data," *Signal Process.*, vol. 100, pp. 169–185, Jul. 2014.
- [43] R. Cogranne, F. Retraint, C. Zitzmann, I. Nikiforov, L. Fillatre, and P. Cornu, "Hidden information detection using decision theory and quantized samples: Methodology, difficulties and results," *Digit. Signal Process.*, vol. 24, pp. 144–161, Jan. 2014.
- [44] T. Qiao, C. Zitzmann, F. Retraint, and R. Cogranne, "Statistical detection of JSteg steganography using hypothesis testing theory," in *Proc. IEEE Int. Conf. Image Process. (ICIP)*, Oct. 2014, pp. 5517–5521.
- [45] T. Qiao, C. Zitzmann, R. Cogranne, and F. Retraint, "Detection of JSteg algorithm using hypothesis testing theory and a statistical model with nuisance parameters," in *Proc. 2nd ACM Workshop Inf. Hiding Multimedia Secur.*, 2014, pp. 3–13.
- [46] T. Qiao, C. Zitzmann, R. Cogranne, and F. Retraint, "Steganalysis of JSteg algorithm using hypothesis testing theory," *EURASIP J. Inf. Secur.*, vol. 2015, no. 1, pp. 1–16, 2015.
- [47] F. de O. Costa, M. Eckmann, W. J. Scheirer, and A. Rocha, "Open set source camera attribution," in *Proc. IEEE 25th SIBGRAPI Conf. Graph., Patterns Images*, Aug. 2012, pp. 71–78.
- [48] F. de O. Costa, E. Silva, M. Eckmann, W. J. Scheirer, and A. Rocha, "Open set source camera attribution and device linking," *Pattern Recognit. Lett.*, vol. 39, pp. 92–101, Apr. 2014.
- [49] H. Yao, T. Qiao, M. Xu, and N. Zheng, "Robust multi-classifier for camera model identification based on convolution neural network," *IEEE Access*, vol. 6, pp. 24973–24982, 2018.
- [50] T. Qiao, F. Retraint, R. Cogranne, and T. H. Thai, "Individual camera device identification from JPEG images," *Signal Process. Image Commun.*, vol. 52, pp. 74–86, Mar. 2017.
- [51] T. Qiao, "Statistical detection for digital image forensics," Ph.D. dissertation, Univ. Technol., Troyes, France, 2016.



TONG QIAO received the B.S. degree in electronic and information engineering from Information Engineering University, Zhengzhou, China, in 2009, and the M.S. degree in communication and information system from Shanghai University, Shanghai, China, in 2012, and the Ph.D. degree from the Laboratory of Systems Modelling and Dependability, University of Technology of Troyes, Troyes, France. Since 2016, he has been an Assistant Professor with the School of Cyberspace, Hangzhou Dianzi University. His current research interests focus on steganalysis and digital image forensics.



FLORENT RETRAINT received the Engineering Diploma degree in computer science from the Compiègne University of Technology in 1993, the M.S. degree in applied mathematics from ENSIMAG in 1994, and the Ph.D. degree in applied mathematics from the National Institute of Applied Sciences of Lyon, France, in 1998. He held a post-doctoral position at CEA Grenoble for one year. He was a Research Engineer with Thomson CSF (Thales S.A) for two years. Since 2002, he has been with the Laboratory of System Modeling and Dependability, Troyes University of Technology. His researches focus on image modeling, statistical image processing, hypothesis testing theory, and anomaly detection and localization.

• • •